Volumetric *in vivo* imaging of intracochlear microstructures in mice by high-speed spectral domain optical coherence tomography

Hrebesh M. Subhash
Viviana Davila
Oregon Health and Science University
School of Medicine
Department of Biomedical Engineering
Biophotonics and Imaging Laboratory
3181 SW Sam Jackson Park Road
Portland, Oregon 97239

Hai Sun
Oregon Health and Science University
School of Medicine
Department of Biomedical Engineering
Biophotonics and Imaging Laboratory
    and
Department of Neurological Surgery
3181 SW Sam Jackson Park Road
Portland, Oregon 97239

Anh T. Nguyen-Huynh
Oregon Health and Science University
School of Medicine
Department of Otolaryngology-Head and Neck Surgery
3181 SW Sam Jackson Park Road
Portland, Oregon 97239

Alfred L. Nuttall
Oregon Health and Science University
School of Medicine
Oregon Hearing Research Center
3181 SW Sam Jackson Park Road
Portland, Oregon 97239

Ruikang K. Wang
Oregon Health and Science University
School of Medicine
Department of Biomedical Engineering
Biophotonics and Imaging Laboratory
    and
Department of Anesthesiology & Peri-operative Medicine
3181 SW Sam Jackson Park Road
Portland, Oregon 97239

Abstract. There is considerable interest in developing new methods for *in vivo* imaging of the complex anatomy of the mammalian cochlea for clinical as well as fundamental studies. In this study, we explored, the feasibility of spectral domain optical coherence tomography (SD-OCT) for 3-D *in vivo* imaging of the cochlea in mice. The SD-OCT system employed in this study used a broadband light source centered at 1300 nm, and the imaging speed of the system was 47,000 A-scans per second using the InGaAs camera. The system was capable of providing fully processed, high-resolution *B*-scan images [512 (axial)×128 (lateral) pixels] at 280 frames per sec. The 3-D imaging acquisition time for a whole cochlea was ∼0.45 sec. The traditional SD-OCT structural imaging algorithm was used to reconstruct 3-D cochlear morphology. We demonstrated that SD-OCT can be successfully used for *in vivo* imaging of important morphological features within the mouse cochlea, such as the otic capsule and structures within, including Reissner's membrane, the basilar membrane, tectorial membrane, organ of Corti, and modiolus of the apical and middle turns. © *2010 Society of Photo-Optical Instrumentation Engineers.* [DOI: 10.1117/1.3456554]

1 Introduction

Hearing loss is one of the most common health problems among the populations of the industrialized world. According to the National Center for Health Statistics, 36 million (17%) of American adults have some degree of hearing loss, making it a public health issue third in line after heart disease and arthritis.[1–3] Hearing loss can be categorized by where or what part of the auditory system is damaged. There are two basic types of hearing loss: conductive hearing loss and sensorineural hearing loss (SNHL).[4] Conductive hearing loss occurs when sound is not conducted efficiently over the outer ear canal, the eardrum, and the tiny bones, or ossicles, of the middle ear to the inner ear. Conductive hearing loss usually involves a reduction in sound level, or a diminished ability to hear faint sounds, that primarily involves the middle ear structures (ossicles or tympanic membrane, or both) or the external ear canal. SNHL occurs when there is damage to the inner ear

Address all correspondence to: Ruikang K. Wang, Oregon Health and Science University School of Medicine, 3181 SW Sam Jackson Park Road, Portland, Oregon 97239. Tel: 503-418-9317; Fax: 503-418-9311; E-mail: wangr@ohsu.edu, or r.k.wang@bme.ogi.edu.

(cochlea) or to the nerve pathways from the inner ear (retro-cochlear) to the brain. Sometimes conductive hearing loss occurs in combination with SNHL. In other words, there may be damage in the outer, middle, or inner ear and the auditory nerve, which is then referred to as mixed hearing loss. Since the structures of the middle and inner ear are difficult to access, there is a need to develop new methodologies for non-invasive imaging of the microanatomy of the cochlea. *In vivo* imaging of intracochlear structures, such as Reissner's membrane, the organ of Corti, and the basilar membrane, could reveal morphological changes associated with inner-ear disorders, like Meniere's syndrome, sudden and subacute SNHL, the presence of a perilymphatic fistula, and certain autoimmune inner ear diseases. *In vivo* imaging of those structures could improve the ability to diagnose and understand these poorly understood disease conditions.

In clinical otolaryngology, a number of *in vivo* imaging modalities have been developed to visualize the microanatomy of the inner ear. Computed tomography (CT) is commonly used to look for gross abnormalities in the bony anatomy of the otic capsule in the areas affected by SNHL, especially when considering congenital malformations.[5] CT is also used to evaluate other bony defects associated with inner-ear pathology, such as superior canal dehiscence syndrome[6] and widened vestibular aqueduct.[7] Magnetic resonance imaging (MRI), particularly with gadolinium enhancement, has been used to diagnose intra- and retro-cochlear pathology as a cause of SNHL, such as by acoustic neuroma[8] and cochlear otosclerosis.[9] The feasibility of high-resolution MRI (HR-MRI) as a diagnostic tool for SNHL, tinnitus, and vertigo has been demonstrated.[10] Functional MRI was also used to study central auditory processing in cochlear implant recipients.[11] Nevertheless, at present neither CT nor MRI has sufficient spatial resolution (on the order of a few millimeters) to visualize the cochlear microanatomy. High-resolution ultrasound imaging [high-frequency ultrasound (HF-US)], >20 MHz, which is a relatively new area of ultrasound imaging, can provide an order of magnitude better imaging resolution than conventional low-frequency ultrasound imaging.[12,13] However, the spatial resolution of HF-US is still limited (60 to 100 μm) when evaluating intracochlear anatomical structures, because it has a shallow penetration depth in bone; the cochlea is located deep in the skull and is surrounded entirely by the dense bone of the otic capsule. Moreover, the acoustic trauma induced by HF-US is another major concern since it may cause damage to the hearing mechanism.

Optical coherence tomography (OCT) is a noninvasive (or minimally invasive), cross-sectional imaging technique that is able to image highly scattering *in vivo* tissue microstructures at a reasonably high spatial resolution between 2 and 20 μm.[14] The principle of OCT is based on optical coherence gating, which can be thought of as an analog to ultrasound B-mode imaging except that light reflected from biological tissue layers is detected rather than acoustic reflections. OCT imaging is performed by directing a focused beam of light into the biological tissue and measuring the delay time (echo delay) for the backscattered light to return to the instrument. Backscatter or reflections are returned from each microstructural feature within the tissue during a single axial (depth) scan. A cross-sectional image of the tissue is constructed by laterally scanning the light beam over the tissue and subse-

quently assembling adjacent axial scans. Early versions of time-domain OCT (TD-OCT) imaging systems achieved notable successes in several areas, but they are limited by relatively low signal-to-noise ratios (SNR) and require long data-acquisition times, so they are not ideal for 3-D *in vivo* imaging.[15] In recent years, frequency-domain optical coherence tomography (FD-OCT), an alternative OCT imaging modality that is also referred to as spectral-domain OCT (SD-OCT), has proven its high speed and high sensitivity for imaging.[16,17] Due to its high sensitivity (<140-dB dynamic range) and its noncontact and noninvasive (minimally invasive) scanning nature, SD-OCT has quickly become an indispensable imaging tool in many fundamental research and clinical applications. High-speed SD-OCT is capable of several tens of thousands of depth scans per second for 3-D *in vivo* imaging of biological specimens. In SD-OCT, the interference pattern in the optical frequency spectrum is analyzed to provide both high-sensitivity and high-speed depth-resolved measurements of the biological specimens. However, the feasibility of high-resolution OCT imaging of the inner ear has not been investigated widely, and only a few studies have previously reported its use for cochlear imaging. Previous OCT inner-ear imaging studies have demonstrated OCT's capability for distinguishing different structural and morphological features of mouse cochlea *in vivo*, *in situ*, and *ex vivo*.[15,18–22] To our knowledge, no publication has addressed the feasibility of OCT for *in vivo* high-resolution 3-D imaging of cochlear microstructures.

2 Materials and Method

2.1 *High-Speed Spectral Domain OCT System*

Figure 1 illustrates the schematic of the high-speed SD-OCT system used in this study, which is similar to one described previously.[23] Briefly, light from a 56-nm-bandwidth, low-coherence broadband infrared superluminescent diode light source (1300 ± 28 nm) was split into two paths in a 10:90 fiber-based Michelson interferometer. One beam was coupled onto a stationary reference mirror, and the second was focused and scanned using a pair of galvo mirrors. The light emerging at the output of the interferometer was sent to a custom-built high-speed spectrometer. The spectrometer consisted of a transmission grating (1175 lines/mm), a camera lens with a focal length of 100 mm, and a 1024-element line scan infrared InGaAs detector with a 25-μm pixel pitch size. The spectral resolution of the designed spectrometer was around 0.141 mm, which provided a total depth range of 3.3 mm in air (2.45 mm in biological tissue by assuming the refractive index of the sample was ~1.35).

One main requirement of the high-speed SD-OCT application is utilization of the camera's full acquisition capability. In our system, the integrating time was set at 17 μs, and the maximum line rate of the camera was 47 KHz. CameraLink™ and a high-speed frame-grabber board (PCI 1428, National Instruments, USA) were used to transfer the raw fringe data from the camera to the host computer. A custom-designed, high-speed software was developed under the Lab VIEW 2009 platform for real-time data acquisition, processing, display, and archiving. The axial resolution of the system was 13 μm in air (~9.6 μm in tissue). We used an objective lens with a 50-mm focal length to deliver the probe beam of
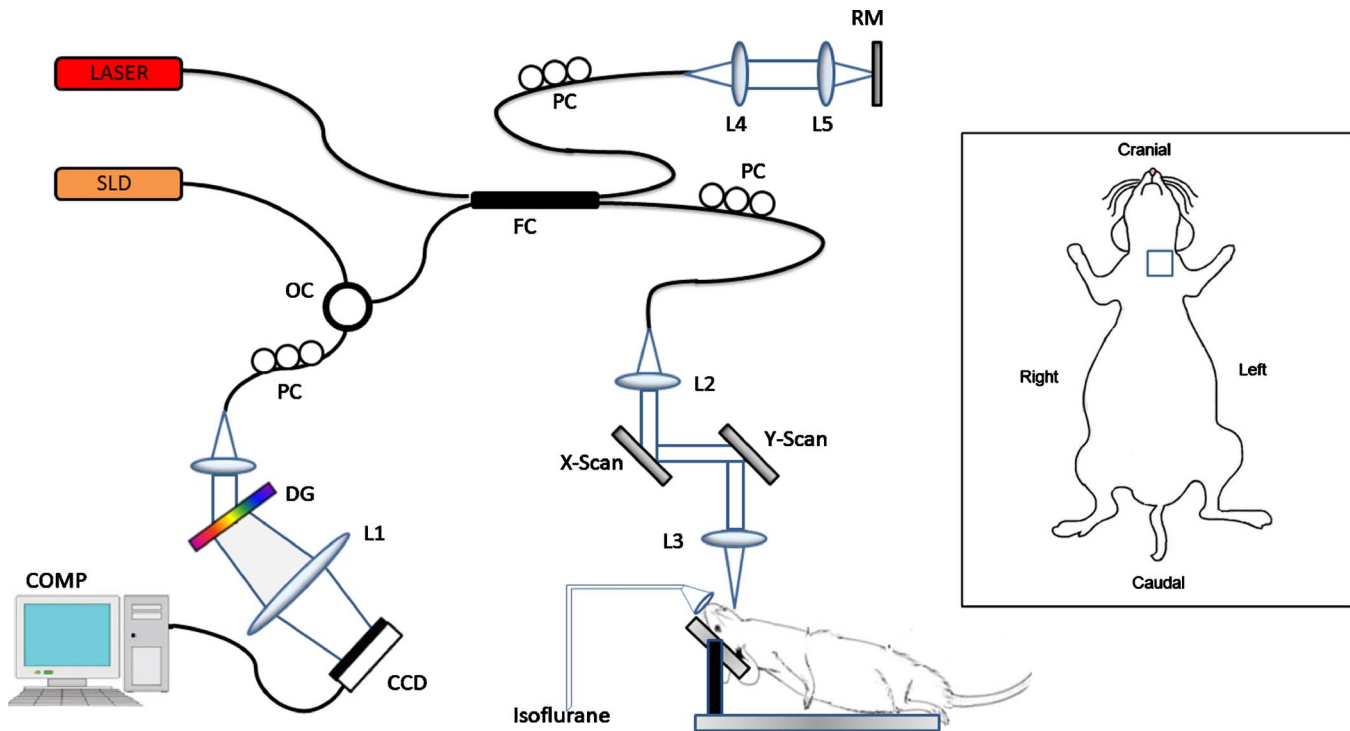
Fig. 1 Experimental setup of high-speed SD-OCT system: SLD=superluminescent diode, OC=optical circulator, FC=10:90 fiber coupler, PC=polarization controller, L1–L5=lenses, RM=reference mirror, LASER=pilot laser for beam guiding, DG=diffraction grating, CCD=line-scan camera, COMP=computer.

4-mm diameter onto the sample, providing a $\sim$16-μm transverse resolution (in tissue) and a $\sim$2-mm depth of focus. The estimated SNR of the system was around 90 dB with a light power on the sample arm at 3 mW.

2.2 Image Acquisition and Reconstruction

For *in vivo* imaging, our imaging protocol provided 3-D cochlear imaging at 280 B-scan frames per second (fps). Each B-scan encompassed a 1.5 mm$\times$2.45 mm (x-z) slice of cochlea. A series of 125 cross-sectional B-scan images were obtained from the medial to lateral direction (1.25 mm), and only $\sim$0.45 sec was required to capture a 3-D volume of 1.5 mm$\times$1.25 mm$\times$2.45 mm ($128\times125\times512$ voxels with a voxel size of $\sim$12$\times$10$\times$10 μm^3) that covered the cochlea.

Before applying the traditional SD-OCT algorithms to reconstruct the OCT images, all the spectral interferograms in each B scan along the x direction were ensemble-averaged at each wavelength to obtain a reference spectrum, which was then subtracted from each A-scan. This operation effectively removed/minimized the autocorrelation, self-cross-correlation, and camera noise artifacts presented in the final OCT images,[24] and considerably improved the image quality. The subtracted spectral interferograms were then converted into the equal frequency space by use of the spline interpolation method, because the spectral interferogram data matrices captured by the CCD camera were functions of wavelength; however, the Fourier transform relationship was between time (distance) and frequency (wavenumber). After scaling the depth range by the refractive index of 1.35 for biological tis-

sue, the reconstructed 2-D OCT images were stacked sequentially to form a 3-D volume with a physical size of 1.5 mm$\times$1.25 mm$\times$2.45 mm ($X\times Y\times Z$).

2.3 Animal Model and Surgical Technique

Since the penetration depth of our OCT system to access the cochlea was limited by the presence of the thick, bony mastoid bulla on the cochlear surface, surgical access to the cochlea was required to visualize the cochlear microstructure. Healthy C57 BL/6 mice weighing around 20 to 30 gm (3 months old) were used in this study. The experimental protocol was in compliance with the federal guidelines for care and handling of small rodents and approved by the Institutional Animal Care and Use Committee (IACUC) of Oregon Health and Science University (OHSU).

Animals were initially anesthetized by a single subcutaneous (s.c.) injection of ketamine (75 mg/kg) and xylazine (10 mg/kg). The mouse was then placed on a heating pad and maintained at 37$\pm$1 °C. Prior to surgically exposing the cochlea, the mouse head was immobilized and positioned onto an imaging platform to minimize the translation of movements due to breathing, which is essential for *in vivo* imaging. The imaging platform was based on a standard mouse stereotaxic instrument.

Under sterile surgical conditions, a ventral incision approach with a longitudinal, paramedian incision was used to access and remove the bone of the tympanic bulla to permit direct access to the inner ear with minimal blood loss or mortality.[25] This approach provided a more direct view of the cochlear turns and round window niche area compared to the
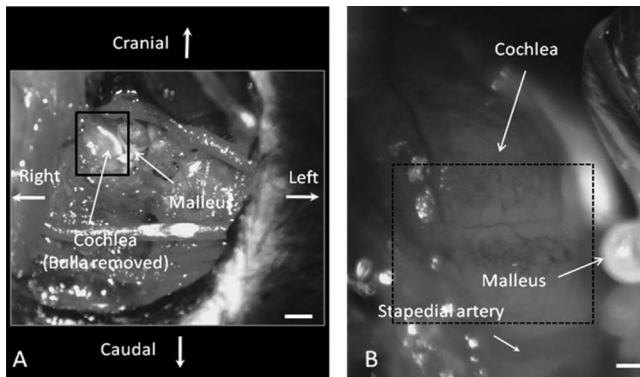
Fig. 2 Surgical view of the left cochlea in mouse. (a) Ventral surgical window through the bulla exposes the middle and basal turns of the cochlea (within the rectangular box). White scale bar=1 mm. (b) Optically magnified view of the exposed cochlea with otic capsule left intact. The dotted rectangle shows the approximate region of the OCT scan. White scale bar=200 μm.

Fig. 3 (a) *In vivo* 2-D cross-sectional OCT image of apical turns of the spiral-shaped cochlea (1.5 mm$\times$2.45 mm). Compare this image with the first frame of Video 1. White bar=250 μm. (b) Optical cross-sectional image using OPFOS.[26] O=otic capsule, M=modiolus, RM =Reissner's membrane, ST=scala tympani, SM=scala media, OC =organ of Corti, and SV=scala vestibuli. White bar=250 μm.

retroauricular approach. After incision, the left submandibular gland and posterior belly of the left digastric muscle were removed by cauterization to reveal a well-defined sterno-cleidomastoid muscle and facial nerve extending anteriorly above the bulla. The bony bulla was exposed, and the dorsal region of the bulla was surgically removed using a micro scissor to provide a clear view of the intact cochlea and the stapedial artery (SA) with its medial margin laying over the edge of the round window niche and coursing anterior-superiorly toward the oval window. After surgery, the anes-thetized mouse with exposed and intact cochlea (Fig. 2) was moved under the beam emanating straight down from the SD-OCT imaging probe for image scanning. During imaging, lo-cal anesthesia with isoflurane (0.2 L/min O$_2$, 0.8 L/min air) was applied, and the breathing interval of the animal was controlled by adjusting the concentration of isoflurane in the vaporizing chamber of the anesthetic station.

3 Results and Discussion

3.1 Results

In vivo OCT images of a portion of the apical, middle, and basal turns of the mouse cochlea were obtained through a surgically prepared opening through the bone of the bulla. Figure 3(a) shows the *in vivo* 2-D OCT cross-sectional image of the cochlea imaged through the intact osseous otic capsule, and Fig. 3(b) shows a standard cochlear cross-sectional im-age, that was imaged using orthogonal-plane fluorescence op-tical sectioning microscopy (OPFOS) described in other publications.[26,27] Figure 4 shows an enlarged view of one of the turns shown in Fig. 3(a). The bony labyrinth of the co-chlea has a spiral shape something like the space inside a snail shell. As shown in Fig. 3, the cochlea consists of relatively large fluid-filled spaces referred to as the scala vestibuli (SV), scala media (SM), and scala tympani (ST). Figure 3(a) also demonstrates that the OCT imaging method is able to detect a wide variety of tissue types ranging from acellular gelatinous material (the tectorial membrane) to dense bone (the otic cap-sule) to the epithelial organ of Corti, which contains the re-markably delicate hair cells.
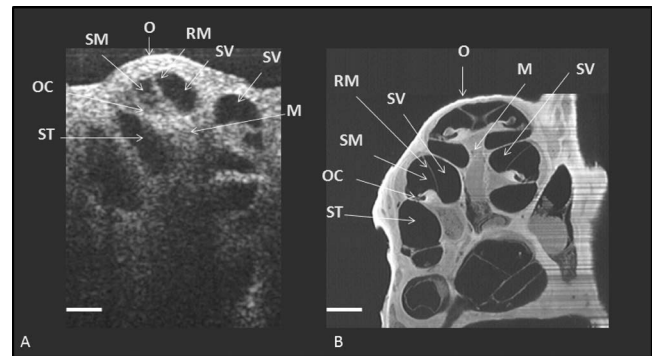
For a better view of the cochlear structures, the 2-D cross-sectional OCT images from the apical to middle turns are shown in Video 1. The cochlea is oriented at a slight angle relative to the imaging beam such that the two cross-sectional halves of the apical turn are seen at the upper right-hand cor-ner at the beginning of the video clip. As the video clip progresses through the cochlea, the right-hand cross-section of the turn ends at the most apical end of the cochlea, called the helicotrema, and the left-hand cross section continues into the middle turn. Figure 5 (Video 2) shows a 3-D volumetric projection image of the cochlear microanatomy obtained by SD-OCT. The dashed line in Fig. 5 indicates the first B-scan. The location of the SA is indicated with the black lines, and the direction of the C-scan is shown with the dotted arrow. To reveal the internal cochlear turns more clearly, the image transparency was increased with 3-D reconstruction software (Amira). As can be seen in both the 3-D OCT image of the cochlea (Fig. 5) and the cross-sectional OPFOS image [Fig. 3(b)], the diameter of each turn becomes progressively smaller from the base to the apex. The cochlear structures exist in a complex, helical geometry spiraling around a central
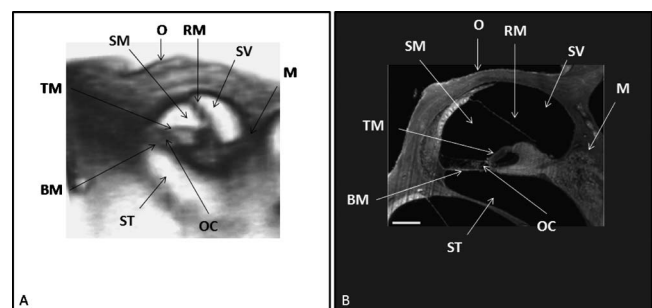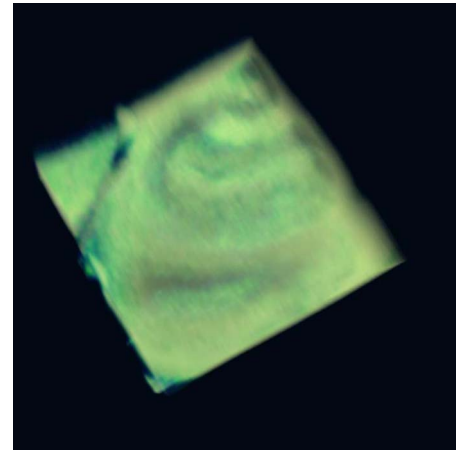

Fig. 4 (a) Enlarged *in vivo* 2-D cross-sectional OCT image of a single apical turn of the cochlea. Both the tectorial membrane (TM) overly-ing the organ of Corti (OC) and the basilar membrane (BM) are visible in this image. (b) Optical sectioning of a single apical turn of the cochlea using OPFOS[27] (reprinted with permission of Elsevier). O =otic capsule, M=modiolus, RM=Reissner's membrane, BM =basilar membrane, ST=scala tympani, SM=scala media, OC =organ of Corti, and SV=scala vestibuli.

Video 1 Flythrough of the 2-D cross-sectional images of the cochlea from the middle to apical turns (QuickTime, 3910.36 KB). [URL: http://dx.doi.org/10.1117/1.3456554.1].

pillar of spongy bone with nerve fibers, the modiolus (M). In comparison with the standard *in vitro* OPFOS image, the OCT cross-sectional image presented here demonstrates a similar microanatomy, both in morphology and scale. For example, the thickness of the organ of Corti (OC) measures approximately 80 μm at its greatest dimension in both the OCT image and the OPFOS image. In addition, the cross-sectional fly-through movie (Video 1) rendered from the 2-D OCT stack images clearly reveals the spiral canal of the cochlea, which is divided lengthwise into three passages (SV, SM, and ST) separated by Reissner's membrane and the basilar mem-

Fig. 5 3-D volumetric projection image of the cochlear microanatomy (Video 2). Dashed line indicates the location of the first B scan. The location of the stapedial artery (SA) is indicated with the back lines, and the direction of the C scan is shown with the dotted arrow.

Video 2 3-D volumetric reconstruction of the cross-sectional OCT images of the apical and middle turns of the cochlea (QuickTime, 185 KB). [URL: http://dx.doi.org/10.1117/1.3456554.2].

brane (BM). The SV and the ST are connected to each other at the helicotrema [Figs. 5, 6(b), and 6(c)].

Figure 4 shows the enlarged, detailed 2-D cross-sectional image of the cochlea imaged with OCT [Fig. 4(a)] in comparison with an OPFOS image [Fig. 4(b)] illustrating the cochlear microanatomy. Figure 6 shows several views of 3-D volume-rendering based on segmentation of OCT data in the sagittal and coronal planes. From the sagittally segmented, 3-D–rendered, and resliced OCT image of the cochlear structure, OCT volume-rendering clearly reveals the cochlear duct (SM) located between Reissner's membrane and the basilar membrane, which can be seen in both Figs. 5 and 6. Figure 6(d) also shows the ability of OCT to visualize the organ of Corti *in vivo*, which resides within the cochlear duct on the basilar membrane. The tectorial membrane is adherent to the organ of Corti in the scala media space. The organ of Corti is a highly organized structure that is responsible for the transduction of mechanical vibrations into neural impulses. The organ of Corti is visible in the 3-D OCT reconstruction [Fig. 6(d)]; however, the detail of individual hair cells within the organ of Corti is beyond the resolution of our present system.
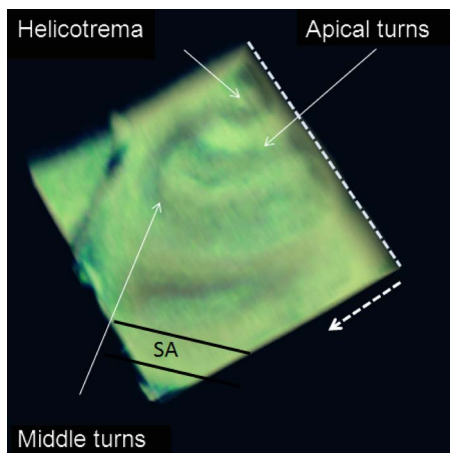
3.2 Discussion

In the present study, the feasibility of high-speed SD-OCT for clear visualization of the inner ear microanatomical features was successfully demonstrated. A tool that provides *in vivo* high-resolution imaging to reveal anatomic and physiological information of the inner ear in a relatively noninvasive and nondestructive manner might shed light on fundamental issues concerning hearing function and loss, enable clinically significant diagnoses, and guide future surgical efforts to restore hearing function by micromanipulation. The results of the current study of *in vivo* imaging of cochlear morphology with high-speed SD-OCT suggest that this imaging modality deserves exploration for such applications.

As an alternative *in vivo* imaging modality for viewing intracochlear structures, SD-OCT has several potential advantages over other cochlear imaging modalities such as CT, MRI, and HR-US. First, SD-OCT is relatively inexpensive and portable. Second, it has the potential to provide real-time
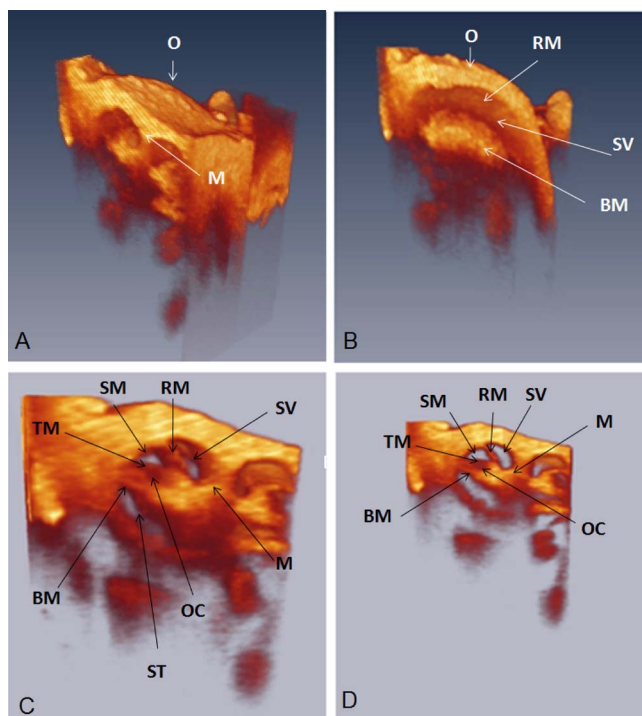
Fig. 6 3-D volume rendering of mouse cochlea, which is segmented and displayed in four different orientations to provide a detailed view of the cochlea. (a) 3-D volumetric image of the entire cochlea imaged. O=optic capsule, M=modiolus. (b) 3-D reconstructed image of the cochlea in the sagittal plane provides an *en face* view of Reissner's membrane and a longitudinal cross-section of the scala vestibuli (SV) and basilar membrane (BM). (c) 3-D reconstruction of the first 50 B frames from the lateral-to-medial direction. (d) 3-D reconstruction of first 25 B frames from the lateral-to-medial direction. Cochlear structures, such as the otic capsule (O), Reissner's membrane (RM), basilar membrane (BM), modiolus (M), scala tympani (ST), scala media (SM), organ of Corti (OC), and scala vestibuli SV are clearly visualized in (c) and (d).

images and can be integrated into surgical guiding tools, such as the endoscope and laryngoscope, which might be very useful for inner-ear intervention in both human subjects and animals. Other current *in vivo* imaging techniques, such as CT and MRI, do not have the sufficient spatial resolution to visualize the microanatomical structures of the cochlea, such as Ressiner's membrane, the basilar membrane, and the organ of Corti. The ability to visualize Ressiner's membrane and the basilar membrane *in vivo* has great importance in both basic scientific research and clinical studies and could be used to understand a wide range of inner ear disorders. For example, endolymphatic hydrops is the result of an enlargement of the endolymphatic fluid space with ballooning of Reissner's membrane and displacement of the basilar membrane. At present, there are no imaging modalities other than OCT that can provide such high-resolution *in vivo* imaging of these cochlear microstructures. The ability of OCT to visualize inner-ear morphologies, such as described above, could change our current understanding of them. However, our current system resolution ($\sim 10~\mu$m) is still not high enough to image individual cellular morphologies within the cochlea. Ultrahigh-resolution OCT (UH-OCT) imaging that uses state-of-the-art broad-bandwidth optical sources, such as femtosec-

ond or supercontinuum lasers, in conjunction with a high numerical aperture (NA) microscopic objective can provide sufficient cellular-level resolution to image the hair cells of the organ of Corti.

Another potential application of OCT is studying the mechanics of sound-wave propagation through the ribbon-shaped BM and how it transduces movement to the cellular and acellular components of the organ of Corti, which are attached to the basilar membrane. *In vivo* imaging also plays a crucial role in cochlear implantation. OCT is feasible for checking the electrode placement in a cochlear implantation. In clinically difficult cases, such as fibrosis in the basal turn or altered anatomy, such as cochlear otosclerosis, it is very relevant to visualize the basilar membrane and the relatively fine position of the cochlear implant to accurately place the electrode.

4 Conclusion

The lack of a high-resolution, noninvasive method for imaging the intracochlear anatomy limits our understanding of cochlear pathology. Clinically, *in vivo* intracochlear imaging would improve the diagnosis of inner-ear disorders. In this paper, we demonstrated the feasibility of using a high-speed SD-OCT system for *in vivo* 3-D imaging of the mammalian cochlear microanatomy with high resolution. This was achieved with the high-speed OCT system working at 1300 nm with an imaging speed at 280 fps that resulted in about 2 volumes per second for imaging a whole cochlea in mice. The spectral selection of a 1300-nm light source also allowed for deeper penetration in highly scattering tissues. We have shown that the high-speed SD-OCT system reported here was capable of clearly visualizing the cochlear microanatomical features such as the otic capsule, Reissner's membrane, basilar membrane, tectorial membrane, modiolus, scala vestibuli, scala media, scala tympani, and organ of Corti. To the best of our knowledge, this is the first demonstration of 3-D *in vivo* imaging of cochlear morphology with SD-OCT.

References

1. http://www.hearingloss.org (accessed January 2010).
2. K. J. Cruickshanks, T. L. Wiley, T. S. Tweed, et al., "Prevalence of hearing loss in older adults in Beaver Dam, Wisconsin. The Epidemiology of Hearing Loss Study," *Am. J. Epidemiol.* **148**(9), 879–886 (1998).
3. P. F. Adams, G. E. Hendershot, and M. A. Marano, "Current estimates from the National Health Interview Survey, 1996," in *Vital Health Statistics*, National Center for Health Statistics, Hyattsville, MD (1999).
4. B. M. Yueh, N. Shapiro, et al., "Screening and management of adult hearing loss in primary care: Scientific review," *J. Am. Med. Assoc.* **289**(15), 1976–1985 (2003).
5. J. W. Casselman, "Diagnostic imaging in clinical neuro-otology,"

Curr. Opin. Neurol. **15**(1), 23–30 (2002).

6. L. B. Minor, J. P. Carey, P. D. Cremer, L. R. Lustig, S. O. Streubel, and M. J. Ruckenstein, "Dehiscence of bone overlying the superior canal as a cause of apparent conductive hearing loss," *Otol. Neurotol.* **24**(2), 270–278 (2003).

7. J. E. McClay, R. Tandy, K. Grundfast, et al., "Major and minor temporal bone abnormalities in children with and without congenital sensorineural hearing loss," *Arch. Otolaryngol. Head Neck Surg.* **128**(6), 664–671 (2002).

8. J. L. Hegarty, S. Patel, N. Fischbein, R. K. Jackler, and A. K. Lalwani, "The value of enhanced magnetic resonance imaging in the evaluation of endocochlear disease," *Laryngoscope* **112**(1), 8–17 (2002).

9. J. P. Goh, L. L. Chan, and T. Y. Tan, "MRI of cochlear otosclerosis," *Br. J. Radiol.* **75**(894), 502–505 (2002).

10. R. Klingebiel, N. Thieme, D. Kivelitz, C. Enzweiler, M. Werbs, and R. Lehmann, "Three-dimensional imaging of the inner ear by volume-rendered reconstructions of magnetic resonance data," *Arch. Otolaryngol. Head Neck Surg.* **128**(5), 549–553 (2002).

11. F. Lazeyras, C. Boex, A. Sigrist, et al., "Functional MRI of auditory cortex activated by multisiteelectrical stimulation of the cochlea," *Neuroimage* **17**(2), 1010–1017 (2002).

12. J. A. Brown, Z. Torbatian, R. B. Adamson, R. Van Wijhe, R. J. Pennings, G. R. Lockwood, and M. L. Bance, "High-frequency *ex vivo* ultrasound imaging of the auditory system," *Ultrasound Med. Biol.* **35**(11), 1899–1907 (2009).

13. J. Mamou, O. Aristizábal, R. H. Silverman, J. A. Ketterling, and D. H. Turnbull, "High-frequency chirp ultrasound imaging with an annular array for ophthalmologic and small-animal imaging," *Ultrasound Med. Biol.* **35**(7), 1198–1208 (2009).

14. D. Huang, E. Swanson, C. Lin, et al., "Optical coherence tomography," *Science* **254**, 1178–1181 (1991).

15. B. J. F. Wong, Y. Zhao, M. Yamaguchi, N. Nassif, Z. Chen, and J. F. De Boer, "Imaging the internal structure of the rat cochlea using optical coherence tomography at 0.827 μm and 1.3 μm," *Arch. Otolaryngol. Head Neck Surg.* **130**(3), 334–338 (2004).

16. A. F. Fercher, W. Drexler, C. K. Hitzenberger, and T. Lasser, "Optical coherence tomography—Principles and applications," *Rep. Prog. Phys.* **66**, 239–303 (2003).

17. P. H. Tomlins and R. K. Wang, "Theory, development and applications of optical coherence tomography," *J. Phys. D* **38**, 2519–2535 (2005).

18. B. J. Wong, J. F. de Boer, B. H. Park, Z. Chen, and J. S. Nelson, "Optical coherence tomography of the rat cochlea," *J. Biomed. Opt.* **5**(4), 367–370 (2000).

19. S. S. Hong and D. M. Freeman, "Doppler optical coherence microscopy for studies of cochlear mechanics," *J. Biomed. Opt.* **11**, 045014 (2006).

20. A. Sepehr, H. R. Djalilian, J. E. Chang, Z. Chen, and B. J. Wong, "Optical coherence tomography of the cochlea in the porcine model," *Laryngoscope* **118**(8), 1449–1451 (2008).

21. N. Choudhury, F. Y. Chen, X. R. Shi, A. L. Nuttall, and R. K. Wang, "Volumetric imaging of blood flow within cochlea in gerbil *in vivo*," *IEEE J. Sel. Top. Quantum Electron.* **15**, 1–6 (2009).

22. J. Lin, H. Staecker, and M. S. Jafri, "Optical coherence tomography imaging of the inner ear: A feasibility study with implications for cochlear implantation," *Ann. Otol. Rhinol. Laryngol.* **117**(5), 341–346 (2008).

23. R. K. Wang and S. Hurst, "Mapping of cerebrovascular blood perfusion in mice with skin and cranium intact by optical microangiography at 1300 nm wavelength," *Opt. Express* **15**(18), 11402–11412 (2007).

24. R. K. Wang and Z. Ma, "A practical approach to eliminate autocorrelation artifacts for volume-rate spectral domain optical coherence tomography," *Phys. Med. Biol.* **51**, 3231–3239 (2006).

25. J. Jero, C. J. Tseng, A. N. Mhatre, and A. K. Lalwani, "A surgical approach appropriate for targeted cochlear gene therapy in the mouse," *Hear. Res.* **151**, 106–114 (2001).

26. Mouse Cochlear Database, University of Minnesota, http://mousecochlea.umn.edu/index.php (accessed January 2010).

27. P. A. Santi, I. Rapson, and A. H Voie, "Development of the mouse cochlea database (MCD)," *Hear. Res.* **243**, 11–17 (2008).